Ramsey Imaging of Optical Traps

Gautam Ramola,[1] Richard Winkelmann,[1] Karthik Chandrashekara,[1] Wolfgang Alt,[1] Peng Xu (许鹏),[1,2] Dieter Meschede,[1] and Andrea Alberti[1,*]

[1] *Institut für Angewandte Physik, Universität Bonn, Wegelerstraße 8, Bonn 53115, Germany*

[2] *State Key Laboratory of Magnetic Resonance and Atomic and Molecular Physics, Innovation Academy for Precision Measurement Science and Technology, Chinese Academy of Sciences, Wuhan 430071, China*

(Received 15 June 2021; revised 4 August 2021; accepted 9 August 2021; published 24 August 2021)

The mapping of the potential landscape with high spatial resolution is crucial for quantum technologies based on ultracold atoms. However, the imaging of optical dipole traps is challenging because purely optical methods, commonly used to profile laser beams in free space, are not applicable in a vacuum. In this work, we demonstrate precise *in situ* imaging of optical dipole traps by probing a hyperfine transition with Ramsey interferometry. Thereby, we obtain an absolute map of the potential landscape with micrometer resolution and shot-noise-limited spectral precision. The idea of the technique is to control the polarization ellipticity of the trap laser beam to induce a differential light shift proportional to the trap potential. By studying the response to polarization ellipticity, we uncover a small but significant nonlinearity in addition to a dominant linear behavior, which is explained by the geometric distribution of the atomic ensemble. Our technique for imaging of optical traps can find wide application in quantum technologies based on ultracold atoms, as it applies to multiple atomic species and is not limited to a particular wavelength or trap geometry.

DOI: 10.1103/PhysRevApplied.16.024041

I. INTRODUCTION

The control of the potential landscape of optical traps is essential for atom-based quantum technologies such as optical-lattice clocks [1], trapped-atom interferometers [2,3], measurement-based quantum computing [4,5], analogue [6,7] and discrete [8] quantum simulators. In these experiments, atoms are trapped in the light field generated either by focused laser beams or with the help of spatial light modulators [9–12] and laser-beam deflectors [13]. At the location of the atoms, the light-field intensity must be known very precisely in order to produce homogeneous [14–17], structured [18–20] and disordered [21,22] potentials, as well as for the sensitive alignment of optical lattices [23] and arrays of microtraps [24,25]. Standard techniques for laser-beam profiling, however, are not suitable for measuring the light-field intensity in a vacuum. Instead, *in situ* information about the trap potential can directly be obtained by probing the atomic ensemble itself, e.g., by measuring motional resonances spectroscopically [26] or by imaging the trapped atom density [27]. These methods estimate the local potential indirectly, as they rely on some additional assumptions (e.g., the geometry of the beams, the harmonic approximation, the thermalization of the atomic ensemble, and the local density approximation) and are not suitable to isolate the contribution of individual beams in setups involving multiple crossed beams.

In contrast, techniques for imaging optical traps aim to directly map the local potential as experienced by the atoms. For alkali-earth atoms, imaging of an optical trap has been demonstrated by measuring the differential light shift induced by the trap laser field upon an ultranarrow optical transition [1]. For species lacking narrow optical transitions, such as alkali atoms, related previous work has shown that the scalar [28] and vector [29] differential light shifts induced by a dipole trap close to resonance can be used to image the local potential, but have not provided an absolute measurement thereof.

In this work, we report on a technique for imaging optical traps with very high precision by probing a hyperfine transition of alkali atoms with position-resolved Ramsey phase tracking. The Ramsey signal measures the differential light shift caused by a small controllable polarization ellipticity of the trap laser beam, which is directly related to the trap potential as experienced by the atoms. By integrating the signal over few repetitions, we attain a spectral precision of about 2 orders of magnitude below the Fourier limit $\nu_F = 1/t$, where t is the interrogation time. Such a high resolution allows us to uncover a nonlinear response of the atomic ensemble to polarization ellipticity, which yields a significant systematic correction to the imaged optical trap. As a result, we obtain an absolute map of the

*alberti@iap.uni-bonn.de

potential landscape at the micrometer scale with an accuracy of the order of 10^{-2} of the maximum potential depth. To exemplify the versatility of the Ramsey imaging technique, we map the dipole potential produced by individual laser beams propagating in diverse directions and with various wavelengths: in between the D doublet (866 nm) and far detuned from it (1064 nm).

II. CONCEPTUAL SCHEME

In an optical dipole trap, the differential light shift between two long-lived states $|a\rangle$ and $|b\rangle$ [Fig. 1(a)] can be written as

$$\delta(\vec{r},\epsilon) = (\eta_s + \eta_v \epsilon) U(\vec{r})/(2\pi\hbar), \tag{1}$$

where $U(\vec{r})$ is the potential experienced by the atoms at position $\vec{r}$ for linear polarization, η_s and η_v are two proportionality factors accounting for the scalar [30] and vector [31] contribution [32], ϵ is the polarization ellipticity of the trap laser beam, and $\hbar$ is the reduced Planck constant. The two factors η_s and η_v only depend on the wavelength λ of the laser beam and the atomic properties, whereas the polarization ellipticity is defined as $\epsilon = (I_R - I_L)/(I_L + I_R)$, where I_L and I_R are the intensities of the left- and right-circular-polarization components of the trap laser beam. To obtain a map of the potential landscape $U(\vec{r})$, we exploit the linear dependence of the light shift $\delta(\vec{r},\epsilon)$ on the ellipticity ϵ, which we can easily vary using a $\lambda/4$ wave plate [Fig. 1(b)]. The light shift is measured precisely with Ramsey interferometry, by tracking the phase shift,

$$\varphi(\vec{r},\epsilon) = 2\pi t \delta(\vec{r},\epsilon), \tag{2}$$

of the Ramsey fringe [Fig. 1(c)] for different values of ϵ.

Alternatively, we can measure the shift $\delta(\vec{r},\epsilon)$ by directly recording a spectrum of the transition. Ramsey interferometry, however, presents the advantage that the model function fitted to the data is known exactly in the form of a sinusoidal fringe. By contrast, direct spectroscopy requires an accurate model of the line shape in order to determine the frequency shift with high precision. The development of such a model is a difficult task because the line shape depends on the detailed dephasing mechanisms acting on the atoms at position $\vec{r}$. Moreover, we remark that direct spectroscopy requires a lengthier data acquisition process compared to Ramsey interferometry to achieve the same statistical uncertainty. In fact, to measure the differential light shift in both the inner and outer regions of the trap precisely, we would need to probe a wide range of detunings, spanning multiple line widths. Conversely, Ramsey interferometry requires only few data points to be measured [e.g., five points in Fig. 1(c)].

To assess the quality of the Ramsey model function, we consider the distribution of the residual mean squares

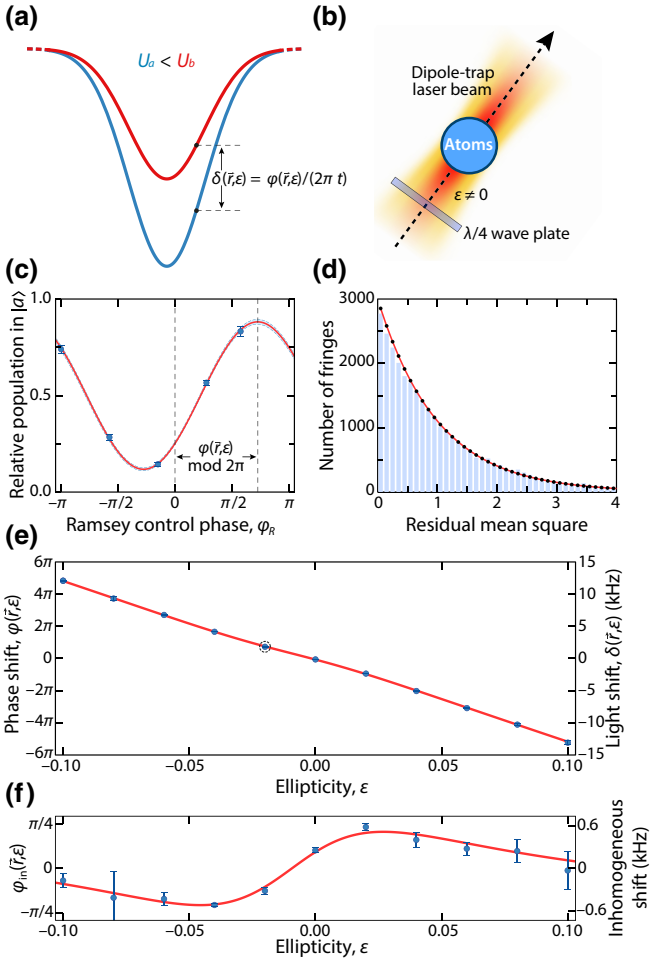

FIG. 1. The imaging of optical potentials by position-resolved Ramsey phase tracking. (a) Atoms in states $|a\rangle$ and $|b\rangle$ experience different trap potentials because of differential light shift [see Eq. (1)]. (b) The trap laser beam to be imaged is made elliptically polarized ($\epsilon \neq 0$) before impinging onto the atomic ensemble. (c) A typical Ramsey interference fringe as a function of the control phase φ_R. (d) The histogram of the residual mean squares derived from fitting the Ramsey fringes recorded for different $\vec{r}$ and ϵ, in excellent agreement with the expected reduced χ^2 distribution (solid line). (e) The Ramsey phase as a function of ϵ measured for a given $\vec{r}$ [see marked pixel in Fig. 2(c)] and a Ramsey duration $t = 200$ μs. On the right-hand y axis, the values are given in frequency units, based on the linear relation in Eq. (2). The circled point is obtained from the Ramsey fringe in (c). (f) The nonlinear contribution to the differential light shift is singled out by subtracting the linear contribution from the data points in (e). The experimental data in (c)–(f) refer to the optical trap produced by the beam called $H3$ (see the text), for which $\eta_s = 2.5 \times 10^{-3}$ and $\eta_v = 1.75$.

derived from fitting $> 10^4$ Ramsey fringes, probed at different locations $\vec{r}$ and for different values of ϵ [Fig. 1(d)]. The comparison with the theoretical χ^2 distribution shows an excellent agreement, validating the interpretation of the estimated fringe parameters as the most likely ones.

Assuming that the dominant noise source is atom shot noise, the uncertainty of the phase obtained from the fit can be expressed as

$$\varphi_{\mathrm{err}}(\epsilon) = \frac{1}{\{[1-\sqrt{1-C(\epsilon)^2}]N\}^{1/2}}, \tag{3}$$

where N is the number of atoms interrogated in the surrounding of $\vec{r}$ and $C(\epsilon)$ is the contrast of the Ramsey fringe, which is a decreasing function of $|\epsilon|$, as shown later. For our measurements with $N \lesssim 500$, we find that the statistical-fit uncertainty on $\varphi(\vec{r},\epsilon)$ is about a factor of 2 greater than $\varphi_{\mathrm{err}}(\epsilon)$. The small excess noise could be explained by atom losses, photon shot noise and, to a lesser extent, by the readout noise of the CCD camera. Based on Eq. (2), the measured phase uncertainty translates into a frequency uncertainty that is about 2 orders of magnitude below ν_F.

The measured Ramsey phase is found to be approximately proportional to the ellipticity ϵ [Fig. 1(e)]. By subtracting the leading linear contribution, a small nonlinearity becomes evident [Fig. 1(f)], which will be discussed in detail later. If we ignore the nonlinear contribution for now, it is straightforward to obtain, by linear extrapolation, the phase $\varphi(\vec{r},\pm 1)$ corresponding to a pure right or left circular polarization, $\epsilon = \pm 1$, and the phase $\varphi(\vec{r},0)$ corresponding to linear polarization. The local trap potential can therefore be expressed as

$$U(\vec{r}) = \pm\frac{\varphi(\vec{r},\pm) - \varphi(\vec{r},0)}{S}, \tag{4}$$

with the factor $S = \eta_v t/\hbar$ playing the role of the sensitivity factor of the Ramsey imaging technique. We remark that the scalar contribution to the differential light shift, $\eta_s U(\vec{r})/(2\pi\hbar)$, has no effect on the reconstructed potential landscape because it does not depend on ϵ.

III. ALKALI ATOMS

We discuss the general case of an alkali atom, with $|a\rangle = |F, m_F\rangle$ and $|b\rangle = |F', m'_F\rangle$ being two hyperfine levels of the electronic ground state. Here, F and F' denote the quantum numbers of the total angular momentum of the atom, whereas m_F and m'_F represent the corresponding magnetic quantum numbers, with the quantization axis aligned in the direction of the laser beam the potential of which we aim to image. Accounting for the vector polarizability [33], we obtain the following expression:

$$\eta_v = (g'_F m'_F - g_F m_F)\frac{\nu_2 - \nu_1}{2(\nu - \nu_1) + \nu - \nu_2}, \tag{5}$$

where g_F and g'_F are the Landé factors of the states $|a\rangle$ and $|b\rangle$, ν_1 and ν_2 are the resonance frequencies of the D_1 and D_2 lines, and $\nu = c/\lambda$ is the frequency of the laser beam, with c being the speed of light.

TABLE I. Reference values of η_v and η_s for a far-detuned dipole trap at 1064 nm for three representative alkali atoms. η_v is calculated for doubly polarized and maximally stretched hyperfine states of the electronic ground state. η_s is much smaller than η_v because it originates from the hyperfine interaction in the electronic ground state.

	^{133}Cs	^{87}Rb	^{23}Na
η_v	-0.16	-0.04	-1×10^{-3}
η_s	1.5×10^{-4}	6.8×10^{-5}	7.8×10^{-6}

Equation (5) shows that the sensitivity factor S is nonzero for all transitions except for clock-type transitions (when $g'_F m'_F = g_F m_F$). Moreover, S increases with the fine-structure splitting, $\nu_2 - \nu_1$, which is larger for heavier atoms (Table I), and for wavelengths closer to one of the two D lines. This behavior is caused by the fact that Ramsey imaging of optical traps works for alkali atoms by leveraging the spin-orbit interaction present in the p orbitals.

IV. EXPERIMENTAL SETUP

We demonstrate Ramsey imaging of optical traps with ^{133}Cs atoms, probing the hyperfine transition between $|a\rangle = |F=3, m_F=3\rangle$ and $|b\rangle = |F=4, m_F=4\rangle$. We map the potential landscape of four optical traps, which are produced by laser beams propagating in different directions and having different wavelengths. Three of the beams (labeled $H1$, $H2$, and $H3$, with $\lambda = 866$ nm) propagate in a horizontal plane, which is perpendicular to the imaging axis, whereas the fourth beam (labeled V, with $\lambda = 1064$ nm) propagates along the vertical direction, which coincides with the imaging axis, and is retroreflected to form an optical standing wave. The four laser beams are overlapped to create a three-dimensional optical lattice, as detailed in Ref. [34].

For each beam the potential of which we intend to map, we make its polarization slightly elliptical by inserting a $\lambda/4$ wave plate in the beam path, as illustrated in Fig. 1(b). The precise value of ϵ can be measured with standard ellipsometry methods, e.g., using a rotating polarizer. As an alternative, in the case of beams $H1$ and $H3$, we use a digital polarization synthesizer [35] to control their ellipticity.

For a fixed value of ϵ, the experimental sequence begins by cooling a cloud of several thousand atoms in a magneto-optical trap. Subsequently, the atoms are transferred into the foregoing three-dimensional optical lattice. The loading procedure is performed in such a way that the atoms are distributed over a relatively large region (60 μm $\times$ 60 μm), covering 90% of the cross section of the laser beams. The atoms trapped in the optical lattice

are then further cooled in all three dimensions to $T \approx 1\ \mu$K by resolved-sideband cooling [36] and simultaneously pumped optically into state $|b\rangle$. Importantly, the bias magnetic field of approximately 3 G, which defines the quantization axis, is rotated adiabatically in the direction of the laser beam to be imaged, by controlling the current flowing through three pairs of compensation coils.

For the Ramsey interferometer, we abruptly turn off all trap laser beams except for the one relevant to the measurement and subsequently use microwave radiation to apply two short $\pi/2$ pulses of 1 μs duration each, separated by a fixed interrogation time $t = 200\ \mu$s. The pulse frequency $\nu_{\rm hfs}$ is chosen to be approximately resonant with the hyperfine transition between $|a\rangle$ and $|b\rangle$ for the atoms occupying the center of the trap. Because of their short duration, the pulses are spectrally broad enough to allow the entire ensemble of atoms to be addressed, including the atoms in the outer regions of the trap, where the differential light shift is much weaker. To avoid systematic phase shifts that could arise in the outer regions of the trap due to slightly off-resonance pulses, we also record for beam $H3$ a reference Ramsey phase map for a vanishing time t, which is then subtracted. For our experimental parameters, this correction is found to be nonsignificant. We also remark that instead of microwave pulses, we could alternatively use optical Raman pulses, since any systematic phase shift caused by spatial intensity inhomogeneity of the intensity of the Raman laser beams can likewise be subtracted.

For the state-selective detection, we remove atoms in state $|b\rangle$ with an optical push-out pulse and then acquire a fluorescence image [37] of the remaining atoms in state $|a\rangle$ through a high-numerical-aperture objective lens [38], which is well suited to resolve the positions of the atoms with high precision. We note that in the absence of an optical lattice, we can employ other imaging techniques (e.g., absorption imaging). The fraction of remaining atoms exhibits a typical Ramsey fringe [Fig. 1(c)],

$$P_a(\vec{r},\epsilon,\varphi_R) = \frac{1}{2} + \frac{C_0}{2}\cos[\varphi'(\vec{r},\epsilon) - \varphi_R], \qquad (6)$$

as we scan φ_R, the relative phase between the two $\pi/2$ pulses. Here, C_0 is the fringe contrast and $\varphi'(\vec{r},\epsilon)$ is a position-dependent phase obtained by tracking the shift of the Ramsey fringe. Considering Eq. (2), we thus find that the measured phase shift $\varphi'(\vec{r},\epsilon)$ directly yields the differential light shift: $\delta(\vec{r},\epsilon) = \varphi'(\vec{r},\epsilon)/(2\pi\, t) + \nu_{\rm hfs} - \nu_{\rm hfs,0}(\vec{r})$, where $\nu_{\rm hfs,0}(\vec{r})$ is the frequency of the hyperfine transition in the absence of light fields. The bare frequency $\nu_{\rm hfs,0}(\vec{r})$ generally varies with $\vec{r}$ due to residual magnetic field gradients but, importantly, does not depend on ϵ. We thus simply use $\varphi'(\vec{r},\epsilon)$ in lieu of $\varphi(\vec{r},\epsilon)$ in Eq. (4) in order to obtain $U(\vec{r})$, without requiring any independent measurement of $\nu_{\rm hfs,0}(\vec{r})$.

V. EXPERIMENTAL RESULTS

The Ramsey signal is analyzed in a position-resolved manner by subdividing the field of view into small pixels. For our analysis, we choose the pixel size $\Delta_P \approx 3.6\ \mu$m, corresponding to 10 pixels of the electron-multiplying CCD camera. Owing to the nonvanishing temperature T, the atoms move during the Ramsey time t on average by approximately 1 μm, which is less than the pixel size Δ_P. We note that for a desired spatial resolution of the potential map, the thermal motion of atoms constrains the maximum allowed Ramsey interrogation time t, which in turn sets the

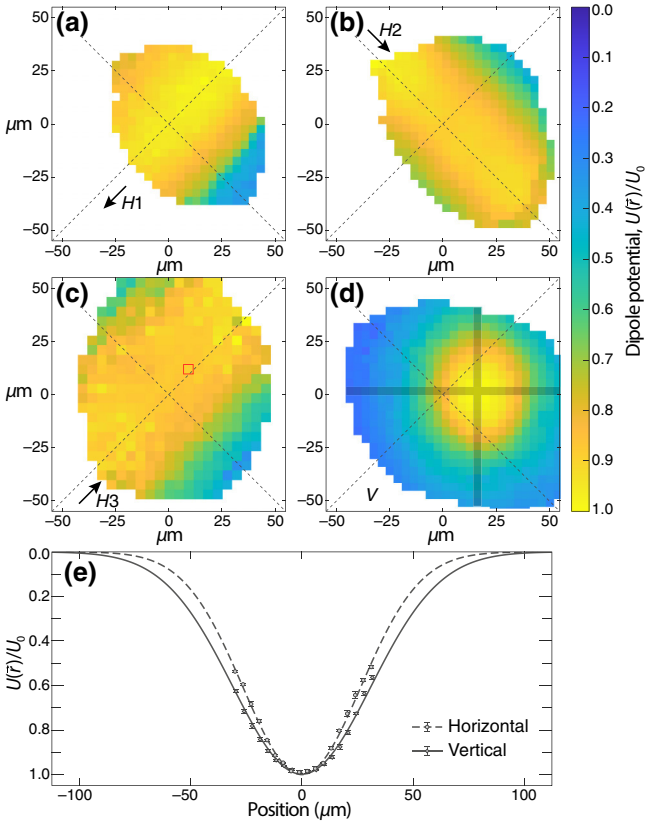

FIG. 2. The Ramsey imaging of four optical traps. The reconstructed potential produced by (a)–(c) three laser beams with $\lambda = 866$ nm propagating in a common horizontal plane and (d) a standing wave with $\lambda = 1064$ nm oriented along the line of sight. The potential is expressed relative to the minimum of the potential, U_0. The dashed lines represent common reference axes. Shown in white are the outer regions where few or no atoms are loaded. The arrows in (a)–(c) indicate the propagation direction of the running-wave laser beams, whereas the marked pixel in (c) corresponds to the data shown in Fig. 1. The potential of the optical lattice resulting from the interference of the laser beams in (a)–(c) is obtained by computing separately the interference pattern of the three beams (not shown here). (e) The data points correspond to two orthogonal cuts as highlighted in (d), whereas the lines are the two Gaussian fitting functions. The slightly different trap waists are likely caused by a small astigmatism of beam V.

Fourier limit ν_F and therefore eventually limits the spectral precision. There is thus a trade-off between the resolvable pixel size Δ_P and Fourier resolution ν_F, where the product of these two quantities is proportional to $\sqrt{k_B T/m}$, where m is the mass of the atoms and k_B is the Boltzmann constant. We also note that any nonzero ellipticity causes a differential force on the states $|a\rangle$ and $|b\rangle$, leading to a displacement between the two wave packets during the interrogation time. Such a displacement may cause a reduction of the contrast C_0 and induce a systematic phase shift. We find, however, that the effect of the differential force is negligible in our case.

Figure 2 shows the potential map for each of the four optical traps, obtained using position-resolved Ramsey phase tracking. Observing the positions of the four reconstructed trap potentials, it is immediately noticeable that the V beam is off center by about 16 μm from the intersection point of the three horizontal beams. A more careful analysis of individual transverse cuts of the mapped potentials shows that the trap waist and the potential depth are determined with an uncertainty of $< 1\%$, whereas the trap transverse position is determined with an uncertainty of a few hundred nanometers. Two orthogonal cuts along the principal axes of beam V are shown in Fig. 2(e) as a representative example, revealing two slightly different trap waists. Such precise geometric information about the position and waist of optical traps is crucial for the sensitive alignment of multiple laser beams in a vacuum and would be hard, if not practically unfeasible, to accomplish using purely optical methods or with indirect *in situ* measurements of the atomic ensemble.

VI. NONLINEAR RESPONSE MODEL

While the linear model in Eq. (1) captures the essence of the Ramsey imaging technique, this model alone is not sufficient to explain the small but significant nonlinear corrections observed as a function of ϵ in Fig. 1(f). We attribute this nonlinear behavior to the distribution of atoms along the direction collinear with the line of sight.

In this direction, the position of atoms cannot be resolved directly by the imaging system. For any given pixel, the detected Ramsey fringe is thus the integrated result of many atoms, each experiencing a slightly different trap laser intensity and, consequently, an inhomogeneous differential light shift. This inhomogeneous differential light shift has a twofold effect on the Ramsey signal: it causes a contrast reduction of the Ramsey fringe and a nonlinear shift, φ_{in}, of the Ramsey phase as a function of ϵ.

To quantitatively model these two effects, we consider a single pixel and assume a one-dimensional Gaussian distribution for the positions of the atoms along the line of sight. The resulting Ramsey fringe is thus obtained by averaging over the ensemble:

$$\int_{-\infty}^{\infty} e^{i\varphi(\vec{r},\epsilon)} p(z - z_0, \sigma) dz = C(\epsilon) e^{i(\eta_s + \eta_v \epsilon) U t/h} e^{i\varphi_{\text{in}}(\epsilon)}, \quad (7)$$

where z is the coordinate along the line of sight, $p(z - z_0, \sigma)$ is a Gaussian function centered at z_0 with width σ, and U is the maximum trap depth along the line of sight, for the pixel considered. To compute the integral in Eq. (7) analytically, we assume that the trap potential along the z direction can be approximated by a harmonic oscillator of angular frequency ω. The computation shows that the phase correction and the contrast can be modeled as follows:

$$\varphi_{\text{in}}(\epsilon) = \frac{\xi(\epsilon)}{1 + \xi(\epsilon)^2} \left(\frac{z_0}{\sqrt{2}\sigma} \right)^2 - \arctan[\xi(\epsilon)], \quad (8a)$$

$$C(\epsilon) = \frac{C_0}{[1 + \xi(\epsilon)^2]^{1/4}} \exp\left[-\frac{\xi(\epsilon)^2}{1 + \xi(\epsilon)^2} \left(\frac{z_0}{\sqrt{2}\sigma} \right)^2 \right], \quad (8b)$$

where $\xi(\epsilon) = (\eta_s + \eta_v \epsilon) m\omega^2 \sigma^2 / (\hbar/t)$ is a dimensionless quantity linear in the ellipticity ϵ. We fit this model

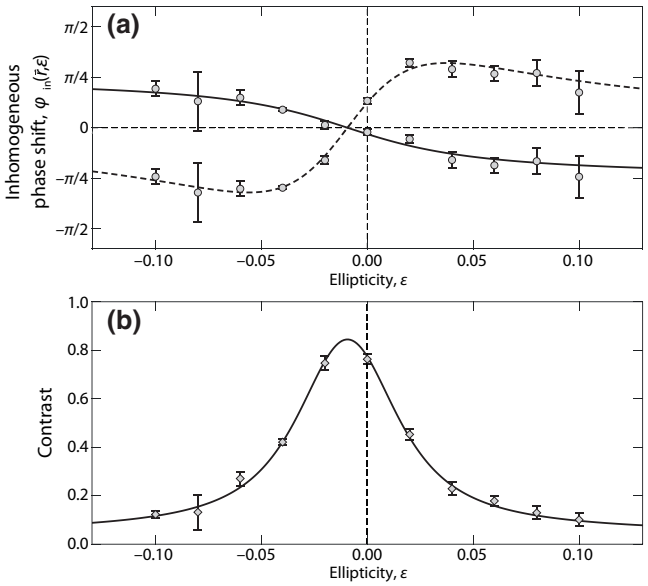

FIG. 3. The nonlinear response of the Ramsey signal to polarization ellipticity ϵ, measured for a single representative pixel, marked in Fig. 2(c). (a) The same data as in Fig. 1(f), showing the nonlinear phase correction. For a close comparison, we display the two nonlinear terms appearing in Eq. (8a) separately by a dashed line (first term) and a solid line (second term). The data points are obtained by subtracting all terms of the fitting model, except for the one of interest. (b) The Ramsey fringe contrast as a function ϵ for the same points in (a), showing a very good agreement with the model in Eq. (8b). An additional ellipticity offset of approximately 0.01 is used to fit the data in (a)–(b), which likely originates from a systemic error in the ellipticity measurement.

simultaneously to both the nonlinear phase contribution [Fig. 3(a)] and the contrast [Fig. 3(b)], which are measured as a function of ϵ for a single representative pixel of beam $H3$. The measured data are in remarkable agreement with the fitting model, from which we obtain that the spread σ is between 10 μm and 15 μm, depending on the pixel position.

Studying the fitting model in Eqs. (8a) and (8b), we recognize that the nonlinear behavior of the phase correction manifests itself only when the fringe contrast C has dropped significantly. It is therefore important to vary ϵ over a sufficiently wide range in order to discriminate the nonlinear correction from the leading linear contribution of Eq. (2). As a result of the nonlinear model, we obtain an absolute map of the potential landscape, which is found to be about 10% deeper than that obtained using the linear model in Eq. (2).

VII. CONCLUSIONS

We demonstrate a technique for the precise imaging of optical trap potentials by Ramsey interferometry. For our demonstration, we map the potential landscape of optical traps for Cs atoms, considering different geometries and wavelengths. Ramsey imaging of optical traps can be applied to other atomic species, such as alkali atoms and magnetic lanthanides [39–41], and to a variety of optical trap geometries (e.g., optical lattices, flat traps, hollow traps, and tailored potentials).

ACKNOWLEDGMENTS

We would like to thank Carsten Robens for helpful discussions. This research was supported by the SFB/TR 185 "Open System Control of Atomic and Photonic Matter" (OSCAR) of the German Research Foundation. G.R. acknowledges support from the Bonn-Cologne Graduate School of Physics and Astronomy. P.X. acknowledges support from the National Key Research and Development Program of China under Grant No. 2016YFA0302800.

[1] G. E. Marti, R. B. Hutson, A. Goban, S. L. Campbell, N. Poli, and J. Ye, Imaging Optical Frequencies with 100 μHz Precision and 1.1 μm Resolution, Phys. Rev. Lett. **120**, 103201 (2018).

[2] N. Poli, F. Y. Wang, M. G. Tarallo, A. Alberti, M. Prevedelli, and G. M. Tino, Precision Measurement of Gravity with Cold Atoms in an Optical Lattice and Comparison with a Classical Gravimeter, Phys. Rev. Lett. **106**, 038501 (2011).

[3] V. Xu, M. Jaffe, C. D. Panda, S. L. Kristensen, L. W. Clark, and H. Müller, Probing gravity by holding atoms for 20 s, Science **366**, 745 (2019).

[4] H. J. Briegel, D. E. Browne, W. Dür, R. Raussendorf, and M. V. den Nest, Measurement-based quantum computation, Nat. Phys. **5**, 19 (2009).

[5] B. Yang, H. Sun, C.-J. Huang, H.-Y. Wang, Y. Deng, H.-N. Dai, Z.-S. Yuan, and J.-W. Pan, Cooling and entangling ultracold atoms in optical lattices, Science **369**, 550 (2020).

[6] I. Bloch, J. Dalibard, and S. Nascimbène, Quantum simulations with ultracold quantum gases, Nat. Phys. **8**, 267 (2012).

[7] A. Browaeys and T. Lahaye, Many-body physics with individually controlled Rydberg atoms, Nat. Phys. **16**, 132 (2020).

[8] M. Sajid, J. K. Asbóth, D. Meschede, R. F. Werner, and A. Alberti, Creating anomalous Floquet Chern insulators with magnetic quantum walks, Phys. Rev. B **99**, 214303 (2019).

[9] A. L. Gaunt and Z. Hadzibabic, Robust digital holography for ultracold atom trapping, Sci. Rep. **2**, 721 (2012).

[10] F. Nogrette, H. Labuhn, S. Ravets, D. Barredo, L. Béguin, A. Vernier, T. Lahaye, and A. Browaeys, Single-Atom Trapping in Holographic 2D Arrays of Microtraps with Arbitrary Geometries, Phys. Rev. X **4**, 021034 (2014).

[11] P. Zupancic, P. M. Preiss, R. Ma, A. Lukin, M. Eric Tai, M. Rispoli, R. Islam, and M. Greiner, Ultra-precise holographic beam shaping for microscopic quantum control, Opt. Express **24**, 13881 (2016).

[12] G. Gauthier, I. Lenton, N. McKay Parry, M. Baker, M. J. Davis, H. Rubinsztein-Dunlop, and T. W. Neely, Direct imaging of a digital-micromirror device for configurable microscopic optical potentials, Optica **3**, 1136 (2016).

[13] K. Henderson, C. Ryu, C. MacCormick, and M. G. Boshier, Experimental demonstration of painting arbitrary and dynamic potentials for Bose-Einstein condensates, New J. Phys. **11**, 043030 (2009).

[14] A. L. Gaunt, T. F. Schmidutz, I. Gotlibovych, R. P. Smith, and Z. Hadzibabic, Bose-Einstein Condensation of Atoms in a Uniform Potential, Phys. Rev. Lett. **110**, 200406 (2013).

[15] J. L. Ville, T. Bienaimé, R. Saint-Jalm, L. Corman, M. Aidelsburger, L. Chomaz, K. Kleinlein, D. Perconte, S. Nascimbène, J. Dalibard, and J. Beugnon, Loading and compression of a single two-dimensional Bose gas in an optical accordion, Phys. Rev. A **95**, 013632 (2017).

[16] B. Mukherjee, Z. Yan, P. B. Patel, Z. Hadzibabic, T. Yefsah, J. Struck, and M. W. Zwierlein, Homogeneous Atomic Fermi Gases, Phys. Rev. Lett. **118**, 123401 (2017).

[17] K. Hueck, N. Luick, L. Sobirey, J. Siegl, T. Lompe, and H. Moritz, Two-Dimensional Homogeneous Fermi Gases, Phys. Rev. Lett. **120**, 060402 (2018).

[18] S. Häusler, S. Nakajima, M. Lebrat, D. Husmann, S. Krinner, T. Esslinger, and J.-P. Brantut, Scanning Gate Microscope for Cold Atomic Gases, Phys. Rev. Lett. **119**, 030403 (2017).

[19] M. Aidelsburger, J. L. Ville, R. Saint-Jalm, S. Nascimbène, J. Dalibard, and J. Beugnon, Relaxation Dynamics in the Merging of N Independent Condensates, Phys. Rev. Lett. **119**, 190403 (2017).

[20] C. Ryu, E. C. Samson, and M. G. Boshier, Quantum interference of currents in an atomtronic SQUID, Nat. Commun. **11**, 3338 (2020).

[21] J.-y. Choi, S. Hild, J. Zeiher, P. Schauß, A. Rubio-Abadal, T. Yefsah, V. Khemani, D. A. Huse, I. Bloch, and C. Gross, Exploring the many-body localization transition in two dimensions, Science **352**, 1547 (2016).

[22] A. Lukin, M. Rispoli, R. Schittko, M. E. Tai, A. M. Kaufman, S. Choi, V. Khemani, J. Léonard, and M. Greiner, Probing entanglement in a many-body-localized system, Science **364**, 256 (2019).

[23] A. Heinz, J. Trautmann, N. Šantić, A. Jihyun Park, I. Bloch, and S. Blatt, Crossed optical cavities with large mode diameters, Opt. Lett. **46**, 250 (2021).

[24] D. Barredo, S. de Léséleuc, V. Lienhard, T. Lahaye, and A. Browaeys, An atom-by-atom assembler of defect-free arbitrary two-dimensional atomic arrays, Science **354**, 1021 (2016).

[25] M. Endres, H. Bernien, A. Keesling, H. Levine, E. R. Anschuetz, A. Krajenbrink, C. Senko, V. Vuletic, M. Greiner, and M. D. Lukin, Atom-by-atom assembly of defect-free one-dimensional cold atom arrays, Science **354**, 1024 (2016).

[26] Y. R. P. Sortais, H. Marion, C. Tuchendler, A. M. Lance, M. Lamare, P. Fournet, C. Armellin, R. Mercier, G. Messin, A. Browaeys, and P. Grangier, Diffraction-limited optics for single-atom manipulation, Phys. Rev. A **75**, 013406 (2007).

[27] S. Wildermuth, S. Hofferberth, I. Lesanovsky, E. Haller, L. M. Andersson, S. Groth, I. Bar-Joseph, P. Krüger, and J. Schmiedmayer, Microscopic magnetic-field imaging, Nature **435**, 440 (2005).

[28] A. Bertoldi, S. Bernon, T. Vanderbruggen, A. Landragin, and P. Bouyer, *In situ* characterization of an optical cavity using atomic light shift, Opt. Lett. **35**, 3769 (2010).

[29] M. Vengalattore, J. M. Higbie, S. R. Leslie, J. Guzman, L. E. Sadler, and D. M. Stamper-Kurn, High-Resolution Magnetometry with a Spinor Bose-Einstein Condensate, Phys. Rev. Lett. **98**, 200801 (2007).

[30] S. Kuhr, W. Alt, D. Schrader, I. Dotsenko, Y. Miroshnychenko, A. Rauschenbeutel, and D. Meschede, Analysis of dephasing mechanisms in a standing-wave dipole trap, Phys. Rev. A **72**, 023406 (2005).

[31] F. Le Kien, P. Schneeweiss, and A. Rauschenbeutel, Dynamical polarizability of atoms in arbitrary light fields: General theory and application to cesium, Eur. Phys. J. D **67**, 92 (2013).

[32] If $|a\rangle$ and $|b\rangle$ have total electronic angular momentum $J \geq 1/2$ (e.g., ground-state levels of magnetic lanthanides), an additional contribution to Eq. (1) originates from the tensor polarizability [31]. This contribution, however, does not dependent on the polarization when the quantization axis is chosen collinear with the laser-beam direction. Therefore, the tensor contribution can be effectively absorbed in η_s.

[33] R. Grimm, M. Weidemüller, and Y. B. Ovchinnikov, Optical dipole traps for neutral atoms, Adv. At., Mol., Opt. Phys. **42**, 95 (2000).

[34] T. Groh, S. Brakhane, W. Alt, D. Meschede, J. K. Asbóth, and A. Alberti, Robustness of topologically protected edge states in quantum walk experiments with neutral atoms, Phys. Rev. A **94**, 013620 (2016).

[35] C. Robens, S. Brakhane, W. Alt, D. Meschede, J. Zopes, and A. Alberti, Fast, High-Precision Optical Polarization Synthesizer for Ultracold-Atom Experiments, Phys. Rev. Appl. **9**, 034016 (2018).

[36] N. Belmechri, L. Förster, W. Alt, A. Widera, D. Meschede, and A. Alberti, Microwave control of atomic motional states in a spin-dependent optical lattice, J. Phys. B: At. Mol. Phys. **46**, 104006 (2013).

[37] A. Alberti, C. Robens, W. Alt, S. Brakhane, M. Karski, R. Reimann, A. Widera, and D. Meschede, Super-resolution microscopy of single atoms in optical lattices, New J. Phys. **18**, 053010 (2016).

[38] C. Robens, S. Brakhane, W. Alt, F. Kleißler, D. Meschede, G. Moon, G. Ramola, and A. Alberti, High numerical aperture (NA = 092) objective lens for imaging and addressing of cold atoms, Opt. Lett. **42**, 1043 (2017).

[39] W. Kao, Y. Tang, N. Q. Burdick, and B. L. Lev, Anisotropic dependence of tune-out wavelength near Dy 741-nm transition, Opt. Express **25**, 3411 (2017).

[40] J. H. Becher, S. Baier, K. Aikawa, M. Lepers, J. F. Wyart, O. Dulieu, and F. Ferlaino, Anisotropic polarizability of erbium atoms, Phys. Rev. A **97**, 012509 (2018).

[41] C. Ravensbergen, V. Corre, E. Soave, M. Kreyer, S. Tzanova, E. Kirilov, and R. Grimm, Accurate Determination of the Dynamical Polarizability of Dysprosium, Phys. Rev. Lett. **120**, 223001 (2018).